

Matrix methods for the design of transconductor ladder filters

N.P.J. Greer, PhD
R.K. Henderson, PhD
Li Ping, PhD
J.I. Sewell, PhD, CEng, FIEE

Indexing terms: Filters, Transconductor ladder

Abstract: Matrix-based methods for the design of transconductor ladder filters are presented. These allow the realisation of any bandpass or lowpass prototype using only one or two values of transconductance. The new methods are illustrated by experimental results from a 1 MHz elliptic lowpass filter, a 400 kHz elliptic bandpass filter, a 400 kHz Chebyshev bandpass filter, and a PLL frequency-control loop, all fabricated in a 1 μm CMOS process.

1 Introduction

In recent years, much research has been directed towards the development of continuous-time transconductor filters [1–7] as an alternative to switched-capacitor (SC) filters [8], particularly in the frequency range 100 kHz to 10 MHz. Although many linear transconductor circuits have been presented in the literature [9–12], less progress has been evident in the development of filter structures that are well suited to transconductor realisation.

A significant problem has been how to design ladder filters without recourse to ratioed transconductances. Ratioed transconductors are undesirable because the transistors which determine the value of a particular transconductor can vary in size within only a small range without suffering from poor matching in one extreme or producing significant parasitic capacitance and high power consumption in the other. Moreover, it is inconvenient for a designer to have to produce a different set of ratioed transconductors for each new filter design. This problem is specific to transconductor filters as the corresponding variables in RC and SC filters (resistors and sampling capacitors, respectively) can be scaled relatively freely.

Most methods used to derive active RC and SC filters from passive prototypes have been based, explicitly or otherwise, on the simulation of nodal voltages and induc-

tor currents [13, 14]. Examples of such filters are leapfrog and coupled-biquad ladders, as well as circuits obtained by simulating inductors using gyrators [15]. These methods have been applied successfully to the design of lowpass transconductor ladders but they cannot generally be applied to bandpass ladders without the use of ratioed transconductor inputs. This is because, when the voltages of a coupled-biquad bandpass filter are scaled for dynamic range, the summing coefficients between biquads take values which are lower than the coefficients within each biquad by a factor typically close to the fractional bandwidth of the filter. The conventional coupled-biquad bandpass structure can only be used for transconductor ladders having an all-pole response of moderate selectivity [16]. The problem described above is compounded for highly selective filters which require large transconductance ratios, and for prototypes containing inductor loops as these lead to noninteger ratios that cannot be implemented by combinations of a unit transconductance [8].

In this paper, we present matrix-based methods for the design of transconductor ladder filters [17, 18], which can be applied to many more response types than conventional techniques. Ladder filters are considered to be preferable to those formed from cascaded biquad stages, the latter typically having much greater passband sensitivity. The objective of this work is to be able to realise any passive ladder as a canonical transconductor filter using only a single value of transconductance, or a small number of values in simple integer ratios.

Similar matrix methods have already been developed for the design of switched capacitor and active RC filters [19, 20]. As well as formalising the design procedure and providing a framework for computer-aided design tools, the use of matrices has facilitated the discovery of superior active filter structures which are not intuitively obvious. The same advantages are found for transconductor filters.

The authors wish to thank Wolfson Microelectronics Ltd. for permission to publish the experimental results. The filters were laid out by Cameron Aitken of Wolfson Microelectronics and fabricated by GEC Plessey Semiconductors. The photomicrographs were taken by Alan Gundlach of Edinburgh University. Financial support was provided by the Department of Trade and Industry (UK) and the Science and Engineering Research Council (UK).

© IEE, 1994

Paper 9721G (E10), first received 17th December 1992 and in revised form 7th June 1993

N.P.J. Greer was with Wolfson Microelectronics Ltd., Edinburgh, EM8 9NX, United Kingdom and is now with Temic MBB Mikrosysteme GmbH, 73230 Kirchheim-Nabern, Germany

R.K. Henderson is with CSEM SA, 2007 Neuchâtel, Switzerland

Li Ping is with Telecom Research Laboratories, Clayton, Victoria 3168, Australia

J.I. Sewell is with the Department of Electrical Engineering, University of Glasgow, Glasgow G12 8LT, United Kingdom

The design procedure can be summarised as follows:

(i) A set of equations (derived by Kirchhoff's laws) which describe the passive prototype are combined to form a matrix equation

$$J = (G + sC + s^{-1}F)V \quad (1)$$

where V is a vector representing the nodal voltages (and/or branch currents), J is a vector representing the input current source and G , C , and F are matrices whose elements are simple algebraic combinations of the passive component values.

(ii) The nodal voltages and branch currents of the prototype can be scaled if required by performing simple multiplication operations upon eqn. 1.

(iii) The second-order matrix equation is decomposed into two first-order design equations by the introduction of a vector of auxiliary variables, X . A large number of decompositions are possible, of which we present those most useful for transconductor filters. The choice of decomposition for a particular filter design is dictated by the type of building block available and the nature of the desired response.

(iv) To form the active filter, each row of each design equation is implemented by a first-order transconductor/capacitor section.

(v) Finally, the filter is scaled in frequency by the appropriate choice of transconductor and capacitor unit values.

2 Matrix representation of the passive prototype ladder

For a given passive prototype ladder, various forms of the second-order matrix equation (eqn. 1) can be constructed, depending on the choice of variables used to form the vector V . We use the terms V -representation, I -representation and VI -representation to refer to the use of nodal voltages, branch currents and mixed variables, respectively, in V . The choice of representation is governed mainly by two factors. First, the order of the matrices (which equals the number of variables in V) should be kept to a minimum so that the resulting active circuit is canonical, i.e. has one integrator per pole of the desired transfer function. Secondly, a representation should be chosen which leads to the matrices G , C and F being as sparse as possible, as the sparsity of these matrices is reflected in the complexity of interconnect in the resulting active circuit.

Each RLC ladder has a 'minimum inductance' and a 'minimum capacitance' version. Identical matrices are obtained if the V -representation is used for the former and the I -representation for the latter. However, the correct representation must be used for a particular prototype to ensure canonicity. Fig. 1 shows the minimum inductance version of a fifth-order elliptic lowpass prototype with 0.28 dB passband ripple and 60.5 dB stopband attenuation. In the V -representation, this ladder is described by the matrices

$$J = \begin{pmatrix} V_{in}/R \\ 0 \\ 0 \end{pmatrix}, \quad V = \begin{pmatrix} V_1 \\ V_2 \\ V_3 \end{pmatrix}, \quad G = \frac{1}{R} \begin{pmatrix} 1 & 0 & 0 \\ 0 & 0 & 0 \\ 0 & 0 & 1 \end{pmatrix},$$

$$C = \begin{pmatrix} C_1 + C_2 & -C_2 & 0 \\ -C_2 & C_2 + C_3 + C_4 & -C_4 \\ 0 & -C_4 & C_4 + C_5 \end{pmatrix}$$

and

$$F = \begin{pmatrix} \frac{1}{L_2} & -\frac{1}{L_2} & 0 \\ -\frac{1}{L_2} & \frac{1}{L_2} + \frac{1}{L_4} & -\frac{1}{L_4} \\ 0 & -\frac{1}{L_4} & \frac{1}{L_4} \end{pmatrix} \quad (2a-e)$$

In general, where the LC pairs in a ladder are parallel, it is best to use the V -representation. As an example, Fig. 2

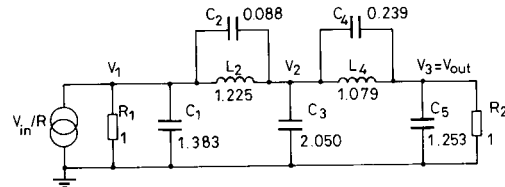


Fig. 1 Fifth-order elliptic lowpass RLC ladder

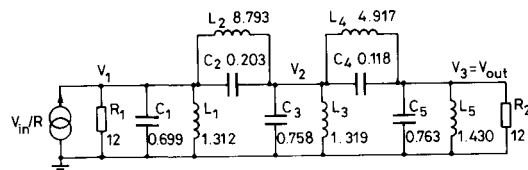


Fig. 2 Sixth-order elliptic bandpass RLC ladder

shows a sixth-order elliptic bandpass prototype with 0.1 dB passband ripple and 50 dB stopband attenuation. In the V -representation this is described by the matrices

$$J = \begin{pmatrix} V_{in}/R \\ 0 \\ 0 \end{pmatrix}, \quad V = \begin{pmatrix} V_1 \\ V_2 \\ V_3 \end{pmatrix}, \quad G = \frac{1}{R} \begin{pmatrix} 1 & 0 & 0 \\ 0 & 0 & 0 \\ 0 & 0 & 1 \end{pmatrix},$$

$$C = \begin{pmatrix} C_1 + C_2 & -C_2 & 0 \\ -C_2 & C_2 + C_3 + C_4 & -C_4 \\ 0 & -C_4 & C_4 + C_5 \end{pmatrix}$$

and

$$F = \begin{pmatrix} \frac{1}{L_1} + \frac{1}{L_2} & -\frac{1}{L_2} & 0 \\ -\frac{1}{L_2} & \frac{1}{L_2} + \frac{1}{L_3} + \frac{1}{L_4} & -\frac{1}{L_4} \\ 0 & -\frac{1}{L_4} & \frac{1}{L_4} + \frac{1}{L_5} \end{pmatrix} \quad (3a-e)$$

Another example is the asymmetric Chebyshev bandpass ladder shown in Fig. 3.

It will be demonstrated in Section 4 that the complexity of a symmetric bandpass transconductor ladder can be reduced if the condition $C = F$ is satisfied. This is the

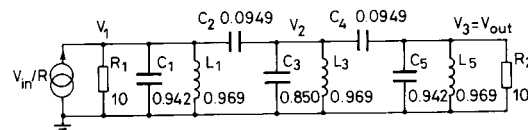


Fig. 3 Sixth-order asymmetric Chebyshev bandpass RLC ladder

case if the bandpass prototype is obtained by transformation of each component of a lowpass ladder individually [13, 14] and if the VI -representation is used. For example, the sixth-order elliptic ladder shown in Fig. 4 is

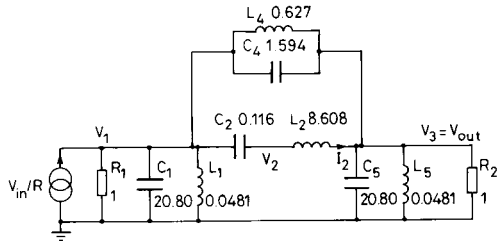


Fig. 4 Another sixth-order elliptic bandpass RLC ladder

obtained by transforming each component of a third-order elliptic prototype. In the VI -representation, this ladder is described by

$$J = \begin{pmatrix} V_{in}/R \\ 0 \\ 0 \end{pmatrix}, \quad V = \begin{pmatrix} V_1 \\ V_{I2} \\ V_3 \end{pmatrix}, \quad G = \frac{1}{R} \begin{pmatrix} 1 & 1 & 0 \\ 1 & 0 & -1 \\ 0 & -1 & 1 \end{pmatrix},$$

$$C = \begin{pmatrix} C_1 + C_4 & 0 & -C_4 \\ 0 & \frac{-L_2}{R^2} & 0 \\ -C_4 & 0 & C_4 + C_5 \end{pmatrix}$$

and

$$\Gamma = \begin{pmatrix} \frac{1}{L_1} + \frac{1}{L_4} & 0 & \frac{-1}{L_4} \\ 0 & \frac{-1}{C_2 R^2} & 0 \\ \frac{-1}{L_4} & 0 & \frac{1}{L_4} + \frac{1}{L_5} \end{pmatrix} \quad (4a-e)$$

To maintain dimensional consistency, the current I_2 is represented by the voltage variable V_{I2} , the multiplying factor being the termination resistance R . In this VI -representation, the C and Γ matrices are identical because by definition $L_i = 1/C_i$.

3 Transconductor-capacitor building blocks

The general first-order transconductor-capacitor building block has the transfer function

$$V_{out} = \left[\sum_i g_i V_i + s \sum_j C_j V_j \right] / sC \quad (5)$$

It is desirable that only one value of g_i be used in a particular filter, but where more than one value is used, they should be in low-integer ratios. Using a conventional transconductor only, eqn. 5 is implemented by the circuit shown in Fig. 5. In this case, the capacitors C_j represent bidirectional coupling paths [21] when driven by internal nodes, as these nodes are all high-impedance. This can be a serious restriction, as many of the techniques available to maintain low-integer capacitor ratios in a filter (Section 4) rely on the use of unidirectional capacitive paths.

To obtain unidirectional capacitive coupling paths, a first-order stage with a low-impedance input and/or output is required. The most obvious realisation of this requires the addition of an opamp to create a virtual earth (Fig. 6). This is expensive in silicon area and current

consumption, particularly as the opamp will need a very high bandwidth for video frequency operation. However,

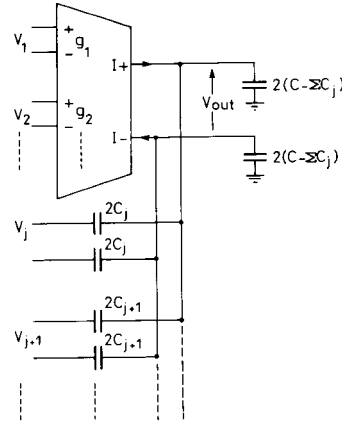


Fig. 5 First-order section using conventional transconductor

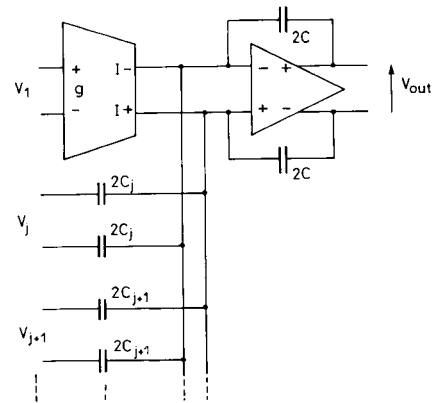


Fig. 6 First-order section with transconductor and opamp

these problems are offset by the fact that the design of the transconductor itself can be somewhat simplified because it is only driving into the virtual earth and does not need a very high output impedance. In the extreme, the transconductor can be reduced to a pair of MOSFETs operating in triode mode, giving a so-called 'MOSFET-C' circuit [22].

An alternative solution is to use a recently reported transconductor with low-impedance inputs [23]. The first-order section using this circuit is shown in Fig. 7.

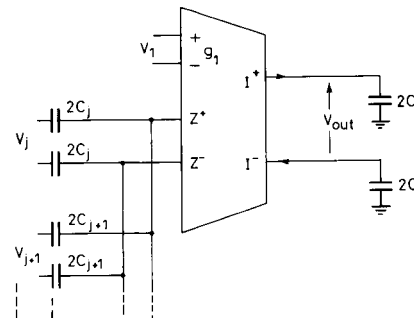


Fig. 7 First-order section using transconductor with low-impedance inputs

The output current of the transconductor is the sum of the transconductance multiplied by the voltage at high-impedance input (V^+ , V^-), and the current entering the low impedance input (Z^+ , Z^-). The circuit diagram of a transconductor with low-impedance inputs is given in Fig. 8.

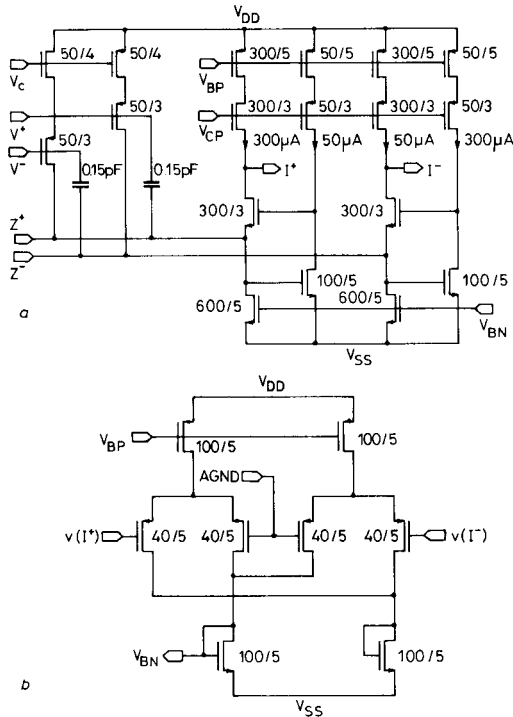


Fig. 8 Folded cascode transconductor with low-impedance inputs (a) and common-mode feedback circuit (b)

4 Matrix decompositions

Five ways of obtaining an active ladder from the general second-order equation (eqn. 1) are now given, together with design examples. The first is recommended for lowpass and the remaining four for bandpass responses. For clarity, single-ended ladders are shown. However, practical transconductor circuits (including those presented in Section 5) are normally fully differential, for several reasons: to obtain linear transconductance functions, to allow the realisation of negative floating capacitors, and to maximise power supply rejection.

In each decomposition, a scaling factor (g or ω_0) is introduced in the definition of the vector X . This factor may be used to perform nodal voltage scaling between the X and V voltages in the transconductor ladder. The scaling of the voltages within each of X and V is determined by the design of the passive prototype. This may also be optimised by matrix techniques, as shown on pages 127–128 of Reference 18.

4.1 Topological decomposition

The Γ matrix is factorised as

$$\Gamma = ADA^T \quad (6)$$

where D is a diagonal matrix whose elements are the reciprocals of the inductances in the prototype (assuming

a V -representation), and A is a conventional incidence matrix. The auxiliary variables are defined by

$$X = (sg)^{-1}DA^T V \quad (7)$$

where g is a scaling factor with the dimensions of conductance, Eqns. 6 and 7 are substituted into eqn. 1 to obtain

$$CV = s^{-1}[J - GV - gAX] \quad (8)$$

Substituting the matrices (eqn. 2a–e) into the design eqns. 7 and 8, and implementing each row with a conventional transconductor stage (Fig. 5) gives the active filter shown in Fig. 9, which is equivalent to a standard leapfrog

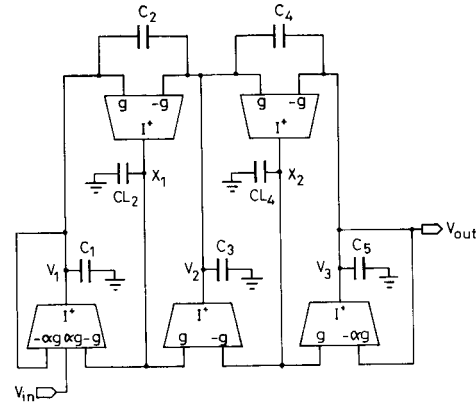


Fig. 9 Lowpass elliptic ladder using conventional transconductor

ladder. Using transconductors with low-impedance inputs instead, we obtain the circuit shown in Fig. 10. The advantage of the first realisation is that there are fewer capacitors and the transconductors are simpler. The advantage of the second is that bottom plates of the floating capacitors can be connected to the low-impedance inputs, so the associated parasitic capacitances do not need to be estimated and subtracted from the grounded capacitors [4].

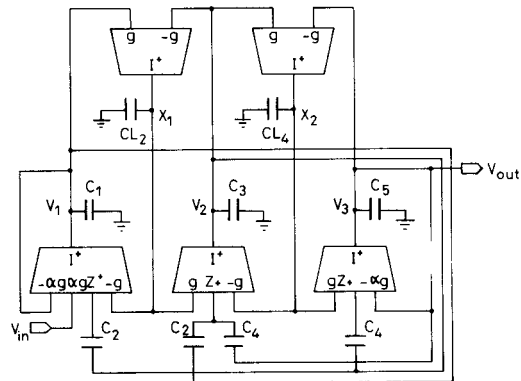


Fig. 10 Lowpass elliptic ladder using transconductor with low-impedance inputs

This topological decomposition is most applicable to lowpass ladders. It is less satisfactory for highly selective bandpass filters, in which case nodal voltage scaling forces high-transconductance ratios, and it cannot be applied to prototypes containing inductor loops as the resulting active circuits are unstable. For bandpass ladders, the following four decompositions are proposed.

4.2 Left-inverse decomposition type 1 (LID1)

The auxiliary variables are defined by

$$gX = sCV \quad (9)$$

where g is again a scaling factor with the dimensions of conductance, and eqn. 9 is substituted into eqn. 1, giving

$$gX = J - GV - s^{-1}\Gamma V \quad (10)$$

The LID1 design equations are obtained by rearranging eqn. 9 and multiplying eqn. 10 by the inverse of Γ :

$$g^{-1}CV = s^{-1}X \quad (11)$$

$$g\Gamma^{-1}X = -s^{-1}V + \Gamma^{-1}[J - GV] \quad (12)$$

From eqns. 11 and 12, the main features of LID1 can be deduced. First, both integrated terms (i.e. those containing the factor s^{-1}) are vectors, so only a single value of transconductance is required in the active ladder. Secondly, both nonintegrated terms on the right-hand side of eqn. 12 are generally asymmetric, so they must be realised using unidirectional capacitive coupling paths. In other words, the dependence of V upon X is not the same as the dependence of X upon V in these terms, so each branch must be realised by a separate capacitor, rather than symmetric branches being realised by a single capacitor connected between the nodes concerned. A single capacitor can be used for symmetric nonintegrated branches arising from off-diagonal terms on the left-hand sides of eqns. 11 and 12, as long as first-order sections with high-impedance outputs are used.

Fig. 11 shows the LID1 realisation of the sixth-order elliptic prototype of Fig. 2. This was obtained by substituting the V -representation matrices, (eqn. 3a-e), into eqns. 11 and 12 and translating each row of each equation into a first-order section of the type shown in Fig. 7.

A general feature of inverse matrix decompositions is that the number of components and the density of interconnect may be high in the transconductor ladder if the sparsity of Γ (or C) is lost upon inversion. This is not a

serious problem for the sixth-order elliptic ladder of Fig. 11, but for higher-order filters care should be taken with the choice of prototype. Essentially this means placing capacitors such that long chains of directly connected inductors are avoided. Some passive prototypes also exist whose Γ matrix may not be inverted at all, due to the determinant being zero. The only examples of such filters known to the authors are bandstop. A question yet to be investigated is to what extent an inverse matrix filter preserves the low-passband sensitivity properties of its passive ladder prototype.

4.3 Left-inverse decomposition type 2 (LID2)

The auxiliary variables are defined by

$$\omega_o X = sV \quad (13)$$

where ω_o is a scaling factor with the dimensions of angular frequency, and eqn. 13 is substituted into eqn. 1, giving

$$\omega_o CX = J - GV - s^{-1}\Gamma V \quad (14)$$

Rearranging eqn. 13 and multiplying eqn. 14 by Γ^{-1} gives the LID2 design equations

$$\omega_o \Gamma^{-1}CX = \Gamma^{-1}J - \Gamma^{-1}GV - s^{-1}V \quad (15)$$

and

$$V = \omega_o s^{-1}X \quad (16)$$

As in the other left-inverse decomposition, only one value of transconductance is required, together with unidirectional nonintegrated paths. The distinguishing feature of LID2 is the term $\Gamma^{-1}C$, which gives the opportunity to obtain a relatively sparse transconductor ladder is a prototype can be used for which $\Gamma = C$. As shown in Section 2, this condition is satisfied for a symmetric bandpass filter derived by the transformation of each component of a lowpass ladder individually. Fig. 12 shows the sixth-order bandpass elliptic transconductor ladder obtained by substituting eqns. 4a-e into eqns. 15

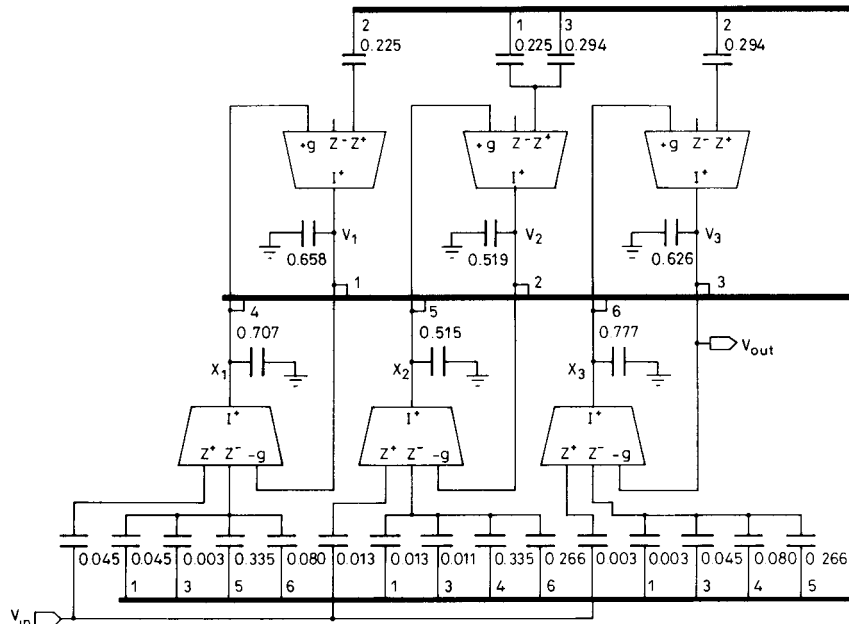


Fig. 11 Elliptic bandpass ladder obtained by L1 decomposition type 1

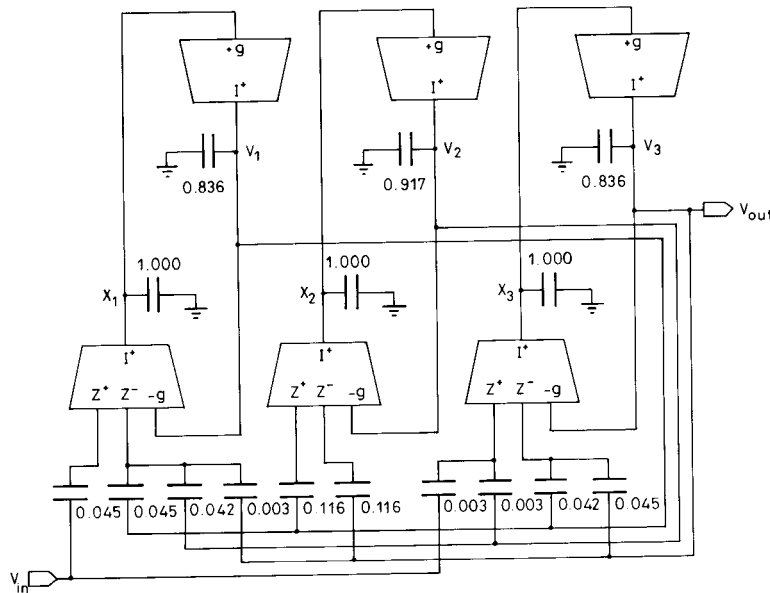


Fig. 12 Elliptic bandpass ladder obtained by LI decomposition type 2

and 16 and implementing each row of each design equation with the first-order section of Fig. 7.

4.4 Right-inverse decomposition (RID)

For the RID, X is defined by

$$gX = s^{-1} \Gamma V \quad (17)$$

This is substituted into eqn. 1 to give

$$J = (G + sC)V + gX \quad (18)$$

The design equations are obtained by multiplying eqn. 17 by Γ^{-1} and rearranging eqn. 18:

$$g\Gamma^{-1}X = s^{-1}V \quad (19)$$

$$g^{-1}CV = s^{-1}[g^{-1}(J - GV) - X] \quad (20)$$

Conventional transconductors can be used to implement eqns. 19 and 20 because the only nonintegrated terms are those arising from the offdiagonal elements of Γ^{-1} and C , which represent bidirectional coupling paths. Neither V nor X is premultiplied before integration, so no unrealisable summing coefficients are introduced. To scale the filter correctly for dynamic range, a second (smaller) value of transconductance is usually required to realise the input branch and filter terminations. This use of a second transconductance value is acceptable because it can be chosen to be in integer ratio to the first and it is used only to represent the termination resistors which are the least sensitive components of the prototype. Such a realisation compares favourably with a coupled-biquad ladder in which high and/or noninteger transconductor ratios can occur throughout the filter.

Fig. 13 shows the RID transconductor ladder obtained from the sixth-order elliptic prototype of Fig. 2, using the V -representation.

4.5 Left-direct decomposition (LD)

The vector of auxiliary variables X is defined by

$$gX = sCV \quad (21)$$

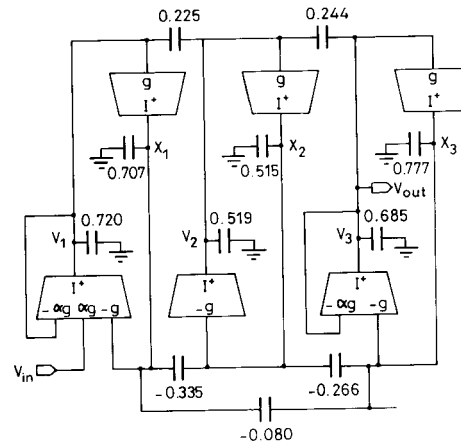


Fig. 13 Elliptic bandpass ladder obtained by RI decomposition

Eqn. 21 is substituted into eqn. 1 to give

$$J = GV + gX + s^{-1} \Gamma V \quad (22)$$

and the design equations are obtained by rearranging eqns. 21 and 22:

$$CV = s^{-1}gX \quad (23)$$

$$X = -(sg)^{-1} \Gamma V - g^{-1}GV + g^{-1}J \quad (24)$$

The principal features of the LD decomposition are as follows. First, the matrix Γ should be diagonal to avoid the requirement for summing integrators which would imply the use of randomly ratioed transconductor values. Secondly, the damping and coupling branches (as represented by the term $g^{-1}GV$) are nonintegrated. These branches are unidirectional, as they describe a dependence of X upon V which is not matched by an identical dependence on V upon X . Therefore, transconductors with low-impedance inputs (Fig. 7) or opamp-based integrators (Fig. 6) must be used in a left-direct filter.

Fig. 14 shows the LD ladder obtained from the sixth-order asymmetric Chebyshev prototype of Fig. 3, using the V -representation. Transconductors with low-impedance inputs are used only for the termination capacitors.

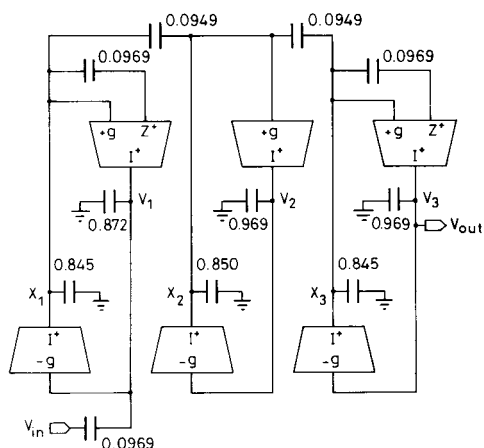


Fig. 14 Chebyshev bandpass ladder obtained by LD decomposition

Left- and right-decomposition filters employ capacitive and resistive damping, respectively, hence we can refer to them as 'E-type' and 'F-type' circuits by analogy with the terminations and terminology used for SC biquads [24].

5 Experimental results

To verify the methods described above, a set of high-frequency transconductor ladder filters has been designed and fabricated on a $1\ \mu\text{m}$ double-poly double-metal CMOS process. In this Section, results are given from three filters: one lowpass elliptic, one bandpass elliptic, and one bandpass Chebyshev. Each of the bandpass filters includes a phase-lock frequency-control loop, a description of which is also given here. The operating frequencies and selectivities of these filters are not high enough for amplitude-control loops [3] to be required.

5.1 Elliptic lowpass filter

Fig. 15 shows the schematic of the experimental lowpass filter, which is a fully differential version of the filter shown in Fig. 9, scaled to a cutoff frequency of 1 MHz. Table 1 summarises the specification and measured performance. Fig. 16 shows the measured amplitude response.

The circuit diagram and a photomicrograph of the double-input transconductor used are shown in Figs. 17

Table 1: Specification and measured performance of lowpass filter

Parameter	Designed	Measured
Order	5	
Cutoff frequency	1 MHz	
Tuning range of cutoff freq.		250 kHz–1.2 MHz
Passband ripple	0.28 dB	0.4 dB
Stopband attenuation	60 dB	61.5 dB
Noise density in passband		97 nV/ $\sqrt{\text{Hz}}$
THD (200 mV rms input)		-67.7 dB
Common mode rejection		71 dB
Power supply rejection		43 dB
Current consumption		10 mA

and 18. The compact layout is achieved by dividing the larger transistors into units $100\ \mu\text{m}$ wide so that the transistors of each polarity can be assembled in rectangular areas, supplied by the respective power lines. Between the two sets of transistors lies a routing bus, which occupies area that would have to be used anyway due to the relatively large 'p-well to n+ diffusion' design rule. The input and output ports run over the VDD line (to the right in the photograph). Including the bias lines in the central bus enables the transconductors to be butted directly. A photomicrograph of the complete lowpass filter is given in Fig. 19. The transconductors are laid out in a single row, and the capacitor bank (with units of 0.5 pF) is shaped to have approximately the same length. Another bus is used to provide efficient routing between the transconductors and capacitors.

5.2 Elliptic bandpass filter

Fig. 20 shows the schematic of the experimental elliptic bandpass filter, which is a fully differential version of the filter shown in Fig. 13, scaled to a centre frequency of 400 kHz. Table 2 summarises the specification and measured performance. Fig. 21 shows the measured amplitude response. A photomicrograph is given in Fig. 22. The noise spike in the stopband at 1.9 MHz is breakthrough from the control loop used to set the centre frequency automatically with respect to a reference clock (see below).

Table 2: Specification and measured performance of elliptic bandpass filter

Parameter	Designed	Measured
Order	6	
Centre frequency	400 kHz	
Tuning range of centre freq.		100 kHz–525 kHz
Bandwidth	10%	10%
Stopband attenuation	50 dB	49.5 dB
Noise density in passband		920 nV/ $\sqrt{\text{Hz}}$
Intermodulation distortion		-43.8 dB
Common mode rejection		72 dB
Power supply rejection		40 dB
Current consumption		11.3 mA

5.3 Chebyshev bandpass filter

Fig. 23 shows the schematic of the experimental Chebyshev bandpass filter. This is a fully differential version of the left-direct filter shown in Fig. 14, scaled to a centre frequency of 400 kHz. To the knowledge of the authors, it is the first example of a transconductor ladder filter that is capacitively terminated and has only a single value of transconductance ($100\ \mu\text{S}$). Table 3 summarises the specification and measured performance. Fig. 24 shows the measured amplitude response. A photomicrograph is given in Fig. 25.

Table 3: Specification and measured performance of Chebyshev bandpass filter

Parameter	Designed	Measured
Order	6	
Centre frequency	400 kHz	
Tuning range of centre freq.		100 kHz–550 kHz
Bandwidth	10%	10%
Noise density in passband		920 nV/ $\sqrt{\text{Hz}}$
Ref. signal breakthrough		200 μV
Intermodulation distortion		-48.7 dB
Common mode rejection		72 dB
Power supply rejection		46 dB
Current consumption		11.6 mA

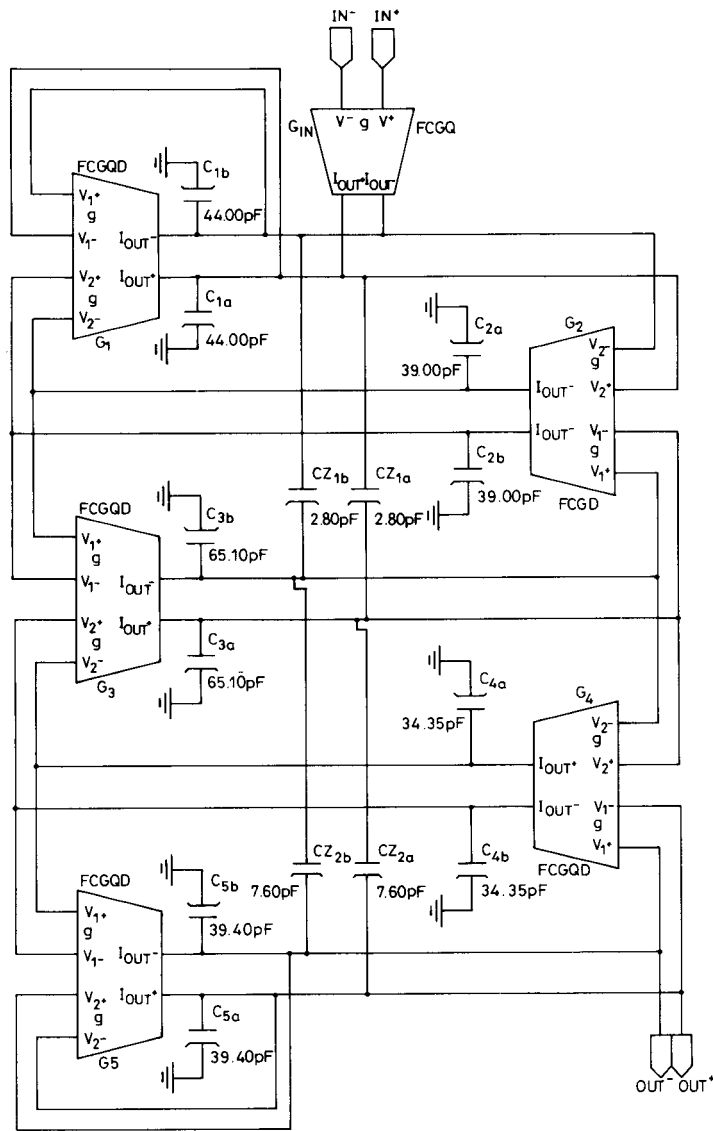


Fig. 15 Fully differential lowpass transconductor ladder filter (bias lines omitted)

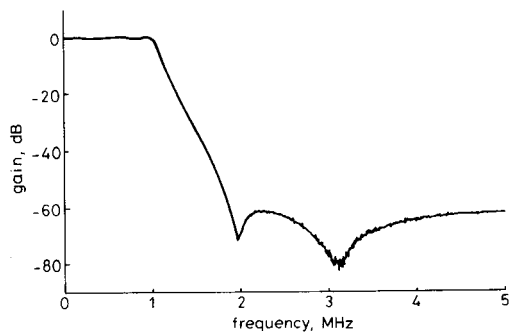


Fig. 16 Measured amplitude response of elliptic lowpass filter

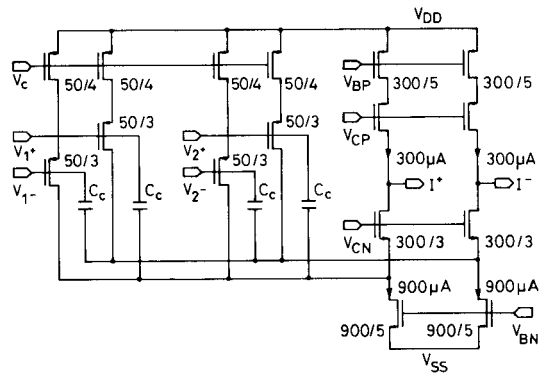


Fig. 17 Schematic of double-input folded cascode transconductor

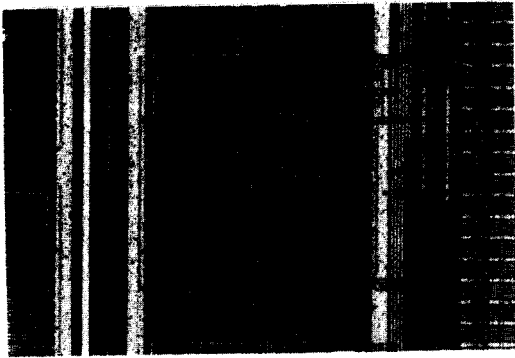


Fig. 18 Photomicrograph of double-input folded cascode transistor

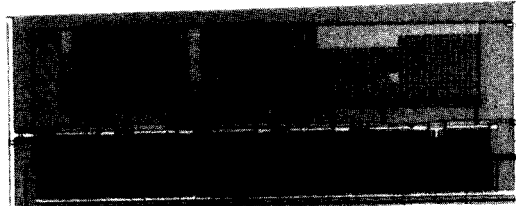


Fig. 19 Photomicrograph of elliptic lowpass filter

5.4 Frequency-control loop

The frequency-control loop fabricated with the test filters is a phase-lock loop (Fig. 26). Based on a voltage-controlled oscillator. This is similar in principle to those described in References 9 and 22, the main difference

being that here a triangle-wave oscillator is used instead of a harmonic oscillator.

The triangle-wave oscillator is illustrated in Fig. 27. An analogue switch selects either $+\Delta V$ or $-\Delta V$ as the input to the transconductor and, respectively, $+\Delta V/2$ or $-\Delta V/2$ as one of the inputs of the comparator. If $+\Delta V$ is selected, the voltage across the capacitor will slew up linearly at a rate $(\Delta Vg/C)$. When this voltage exceeds $\Delta V/2$, the comparator changes state so that the output of the analogue switch changes to $-\Delta V$. Then the output of the transconductor slews down until its value reaches $-\Delta V/2$ and the comparator changes state again. In each

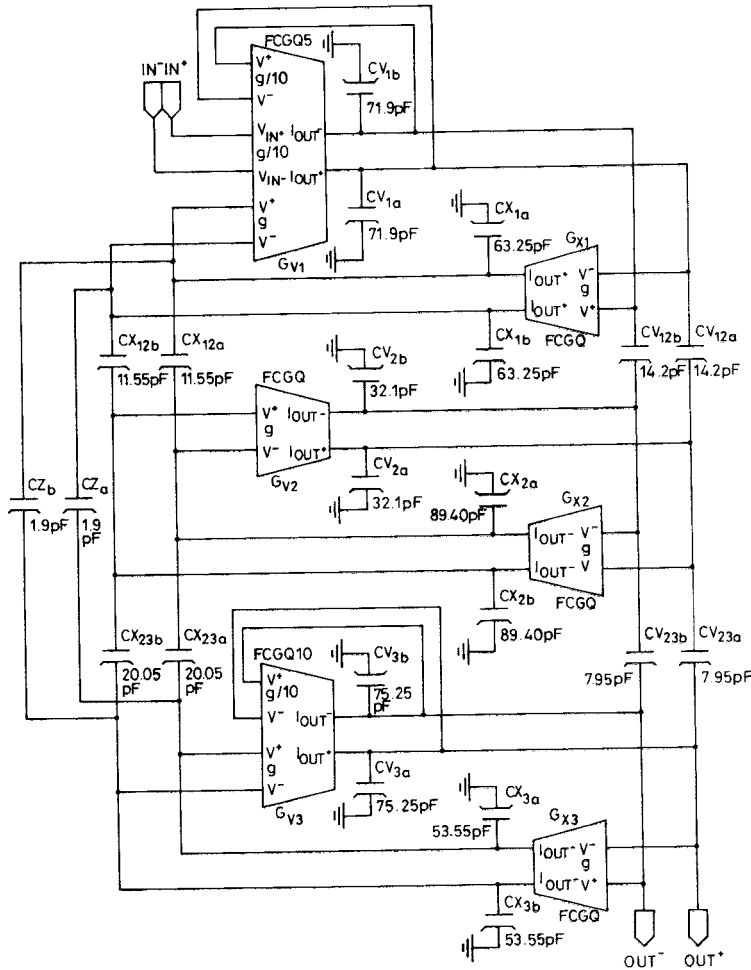


Fig. 20 Fully differential elliptic bandpass filter (bias lines omitted)

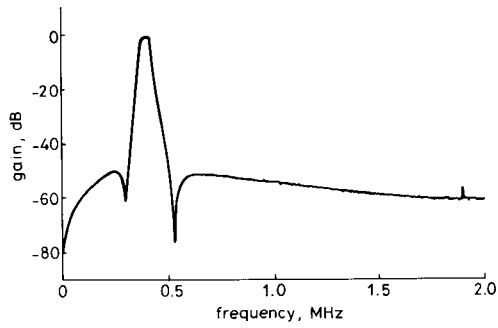


Fig. 21 Measured amplitude response of elliptic bandpass filter

period, the transconductor output has to slew twice through a range of magnitude ΔV , so the frequency of oscillation is

$$f_{osc} = \frac{\Delta V g / C}{2 \Delta V} = \frac{g}{2C} \quad (25)$$

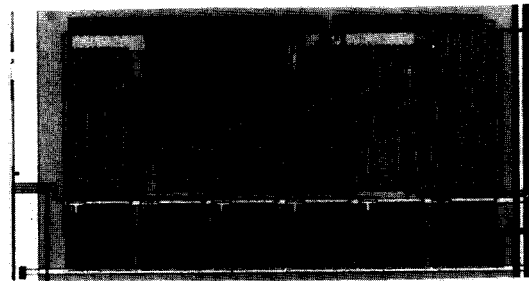


Fig. 22 Photomicrograph of elliptic bandpass filter

The output of the comparator is, of course, a square wave at the same frequency.

The phase of the VCO output is compared to that of a reference square-wave clock by an XOR gate followed by a single-order lowpass filter. The result of the phase comparison is used as the control voltage for the transconductor in the VCO. When the PLL reaches lock, the

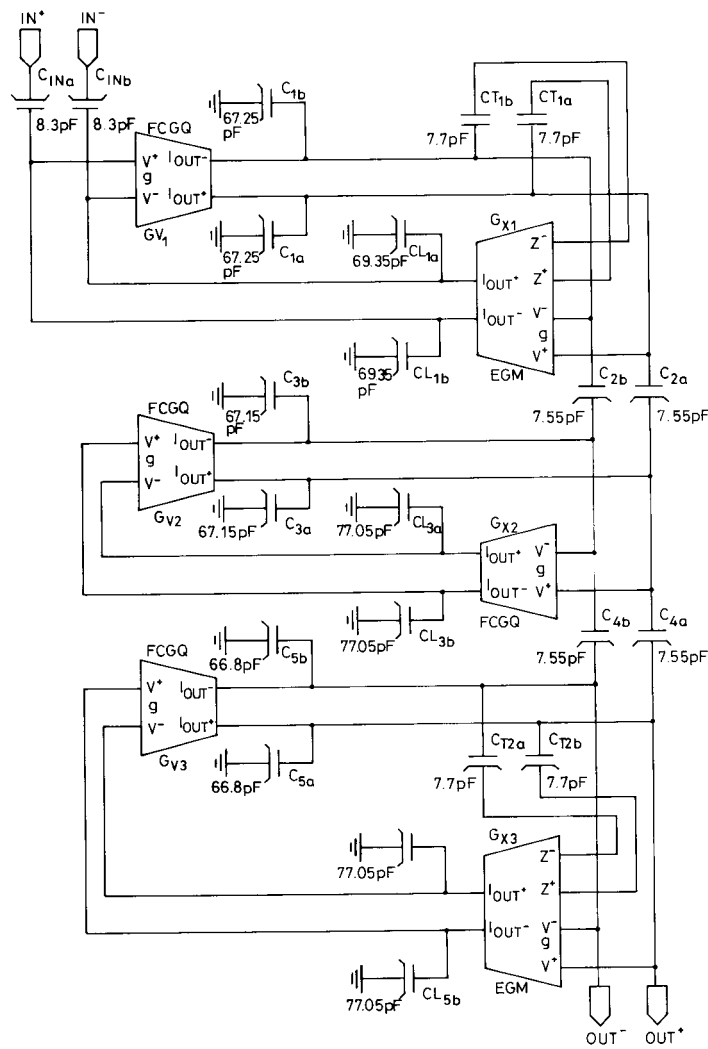


Fig. 23 Fully differential Chebyshev bandpass filter (bias lines omitted)

reference and VCO frequencies are identical, and so according to eqn. 25 the time constant of the trans-conductor and capacitor in the VCO are set. The same control voltage is used for each transconductor in the 'slave' filter. Therefore, within the accuracy of trans-conductor and capacitor matching, the frequency response of the filter is scaled with respect to the reference clock.

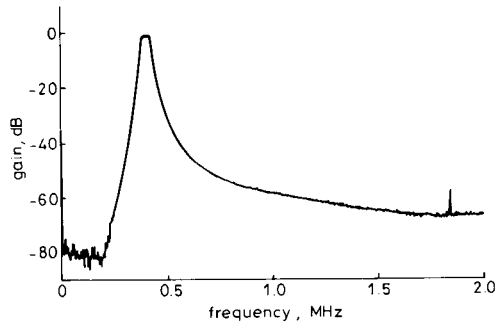


Fig. 24 Measured amplitude response of Chebyshev bandpass filter

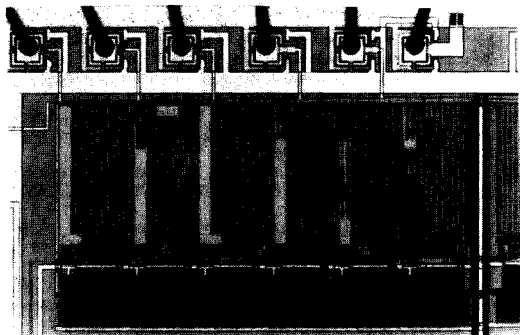


Fig. 25 Photomicrograph of Chebyshev bandpass filter

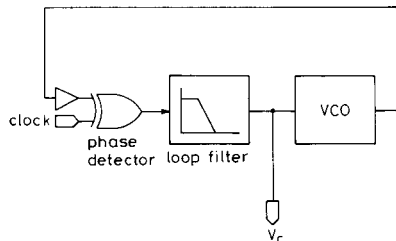


Fig. 26 PLL control loop

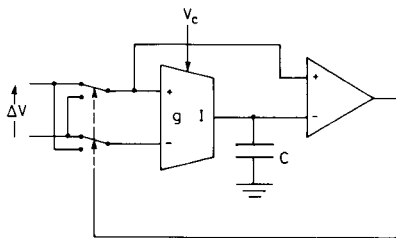


Fig. 27 Triangle-wave voltage-controlled oscillator

The operation of the control loop is illustrated in Fig. 28 which shows the measured amplitude response of the elliptic bandpass filter for three different values of clock frequency (865 kHz, 965 kHz and 1.065 MHz).

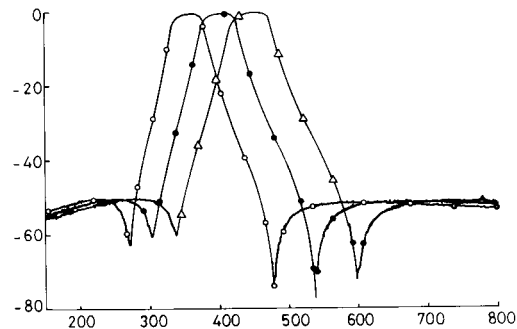


Fig. 28 Measured elliptic bandpass filter response for three values of reference clock frequency

□ 865 kHz
■ 965 kHz
◇ 1.065 MHz

6 Conclusions

A matrix-based methodology for the design of trans-conductor ladder filters has been presented. Many alternative design routes are possible, depending upon: how

Table 4: Comparison of different representations of RLC prototype

Name	Variables of prototype used	Comments
V	voltages	Best for a 'minimum inductance' prototype containing only parallel LC pairs
VI	voltages and currents	Best when prototype contains both parallel and series LC pairs
I	currents	Best for a 'minimum capacitance' prototype containing only series LC pairs

Table 5: Comparison of different decompositions of second-order matrix equation

Name (acronym)	Defining equations	Comments
Topological (TD)	7, 8	Most applicable to lowpass filters. When conventional transconductors are used, gives standard leapfrog filters
Left-inverse type 1 (LID1)	11, 12	Applicable to any bandpass filter. Only one value of transconductance needed per filter. Requires transconductor stages with unidirectional nonintegrating paths
Left-inverse type 2 (LID2)	15, 16	Similar to LID1, but gives sparser active circuit if a prototype is used, for which the condition $\Gamma = C$ is satisfied
Right-inverse (RID)	19, 20	Applicable to any bandpass filter. Conventional transconductors may be used, with up to two values required
Left-direct (LD)	23, 24	Applicable to all-pole bandpass filters. Only one value of transconductance needed per filter. Requires transconductor stages with unidirectional nonintegrating paths

Table 6: Comparison of different first-order transconductor stages

Active circuit used	Comments
Conventional transconductor (Fig. 5)	Best for VHF, due to simplicity. Unidirectional nonintegrating paths are not available. Parasitic input and output capacitance must be compensated for.
Opamp plus conventional transconductor or MOSFET 'resistor' (Fig. 8)	Parasitic capacitance does not affect filter, to first order. Presence of low-impedance nodes makes unidirectional paths available. Opamp dominant pole must be much higher in frequency than filter poles
Transconductor with low-impedance inputs (Fig. 7)	Combines good high-frequency performance of conventional transconductor with usefulness of unidirectional paths. But parasitic capacitances have first-order effect

the prototype ladder is represented by a second-order matrix equation, the way this equation may be decomposed into first-order equations, and the type of transconductor stage that is used to realise the first-order equation. The choices available and their relative merits are summarised in Tables 4 to 6. The utility of the techniques described is demonstrated by results from three high-frequency CMOS transconductor ladder filters.

7 References

- TAN, K.S., and GRAY, P.R.: 'Fully integrated analog filters using bipolar-JFET technology', *IEEE J. Solid-State Circuits*, 1978, SC-13, (6), pp. 814-821
- CHIOU, C.-F., and SCHAUMANN, R.: 'Design and performance of a fully integrated bipolar 10.7-MHz analog bandpass filter', *IEEE Trans. Circuits Syst.*, 1986, CAS-33, pp. 116-124
- PARK, C.S., and SCHAUMANN, R.: 'Design of a 4 MHz analog integrated CMOS transconductance-C bandpass filter', *IEEE J. Solid-State Circuits*, 1988, SC-23, pp. 987-996
- PENNOCK, J., FRITH, P.J., and BARKER, R.G.: 'CMOS triode transconductor continuous time filters'. Proc. IEEE custom integrated circuits conf., 1986, pp. 378-381
- NAUTA, B.: 'CMOS VHF transconductance-C lowpass filter', *Electron. Lett.*, 1990, 26, (7), pp. 421-422
- SANCHEZ-SINENCIO, E., GEIGER, R.L., and NEVAREZ-LOZANO, H.: 'Generation of continuous-time two integrator loop OTA filter structures', *IEEE Trans. Circuits Syst.*, 1988, CAS-35, pp. 936-946
- TAN, M.A., and SCHAUMANN, R.: 'Simulating general-parameter LC-ladder filters for monolithic realizations with only transconductance elements and grounded capacitors', *IEEE Trans. Circuits Syst.*, 1989, CAS-36, (2), pp. 299-306
- CHOI, T.C., KANESHIRO, R.T., BRODERSON, R.W., GRAY, P.R., JETT, W.B., and WILCOX, M.: 'High-frequency CMOS switched-capacitor filters for communications application', *IEEE J. Solid-State Circuits*, 1983, SC-18, pp. 652-664
- KRUMMENACHER, F., and JOEHL, N.: 'A 4 MHz CMOS continuous-time filter with on-chip automatic tuning', *IEEE J. Solid-State Circuits*, 1988, SC-23, (3), pp. 750-758
- NEDUNGADI, A.P., and VISWANATHAN, T.R.: 'Design of linear CMOS transconductance-elements', *IEEE Trans. Circuits Syst.*, 1984, CAS-31, (10), pp. 891-894
- SEEVINCK, E., and WASSENAAR, R.F.: 'A versatile CMOS linear transconductor/square-law function circuit', *IEEE J. Solid-State Circuits*, 1987, SC-22, (3), pp. 366-377
- WANG, Z., and GUGGENBUHL, W.: 'A voltage-controllable linear MOS transconductor using bias offset technique', *IEEE J. Solid-State Circuits*, 1990, SC-25, (1), pp. 315-317
- VAN VALKENBURG, M.E.: 'Analog filter design' (Holt Saunders, New York, 1982)
- SAAL, R., and ENTENMANN, W.: 'Handbook of filter design' (AEG-Telefunken, Berlin and Frankfurt, 1979)
- MOULDING, K., QUARTLY, J.R., RANKIN, P.J., THOMPSON, R.S., and WILSON, G.A.: 'Gyrator video filter IC with automatic tuning'. Proc. IEEE ISSCC, 1980, pp. 86-87
- KRUMMENACHER, F., and VAN RUYMBEKE, G.: 'Integrated selectivity for narrow-band FM IF systems', *IEEE J. Solid-State Circuits*, 1990, SC-25, (3), pp. 757-760
- GREER, N.P.J., HENDERSON, R.K., PING, L., and SEWELL, J.I.: 'Matrix methods for the design of transconductor ladder filters'. Proc. IEEE ISCAS, Singapore, June 1991, pp. 1355-1358
- GREER, N.P.J.: 'The design of high frequency transconductor ladder filters'. PhD thesis, University of Edinburgh, 1992
- PING, L., HENDERSON, R.K., and SEWELL, J.I.: 'A methodology for integrated ladder filter design', *IEEE Trans. Circuits Syst.*, 1991, CAS-38, (8), pp. 853-868
- PING, L., and SEWELL, J.I.: 'The LUD approach to switched-capacitor filter design', *IEEE Trans. Circuits Syst.*, 1987, CAS-34, (7), pp. 1611-1614
- KHORRAMABADI, H., and GRAY, P.R.: 'High-frequency CMOS continuous-time filters', *IEEE J. Solid-State Circuits*, 1984, SC-19, pp. 939-948
- BANU, M., and TSIVIDIS, Y.: 'An elliptic continuous-time CMOS filter with on-chip automatic tuning', *IEEE J. Solid-State Circuits*, 1985, SC-20, (6), pp. 1114-1121
- GREER, N.P.J., and DENYER, P.B.: 'New folded cascode transconductor for bandpass ladder filters', *IEE Proc. G, Circuits Devices Syst.*, 1991, 138, (5), pp. 551-556
- FLEISCHER, P.E., and LAKER, K.R.: 'A family of active switched capacitor biquad building blocks', *Bell Syst. Tech. J.*, 1979, 58, pp. 2235-2269